

# Observation of astrophysically-relevant superadiabaticity in a plasma confined by a dipole magnet

Ayesha Nanda<sup>a)</sup> and Sudeep Bhattacharjee<sup>b)</sup>

Department of Physics, Indian Institute of Technology Kanpur, Kanpur, Uttar Pradesh - 208016, India

(Dated: 18 October 2024)

The polytropic index of electrons in a magnetized plasma is experimentally investigated in the presence of heating and anisotropic work done, incorporating the effective dimensionality arising from temperature anisotropy. The study is performed in a plasma confined by a permanent cylindrical dipole magnet using a compact device. The measurements clearly demonstrate localized regions of superadiabatic electrons due to particle acceleration and energization through non-resonant heating processes. The realization of superadiabaticity is universal where heating dominates the work done and has broader implications for energy exchange processes in space and astrophysically-relevant plasmas.

Thermodynamic methods have been extensively applied in plasmas to investigate the exchange of heat, energy, and work<sup>1</sup>. The polytropic index ( $\gamma$ ) is an important parameter that characterizes compression or expansion and the associated heat transfer processes<sup>2</sup>, and has been the subject of extensive investigation in space and laboratory plasmas<sup>3-6</sup>. The polytropic index varies widely, for example, astrophysical plasmas can have  $\gamma < 1$ <sup>7</sup>, or  $\gamma$  close to the adiabatic index  $\gamma_a (= 1 + 2/f$ , where  $f$  is the kinetic degrees of freedom)<sup>8</sup>,  $\gamma$  can also be within the subadiabatic range ( $1 < \gamma < \gamma_a$ )<sup>9</sup> or even be superadiabatic ( $\gamma > \gamma_a$ )<sup>3</sup>. In contrast, laboratory experiments typically yield polytropic indices that range from isothermal ( $\gamma = 1$ ) to adiabatic index, thus  $\gamma \in [1, \gamma_a]$ <sup>10-13</sup>. The pictorial illustration of the polytropic index spectrum as per current understanding is shown in Fig. 1.

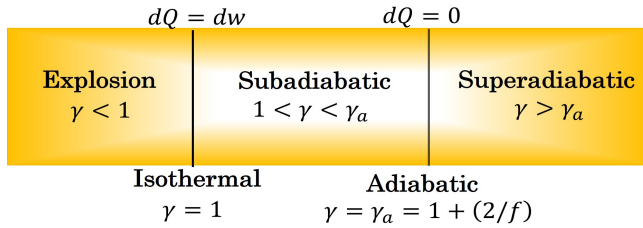


FIG. 1. Illustration of the polytropic index spectrum:  $dQ$  is the heat applied and  $dw$  is the work done.

In all the aforementioned works, the polytropic index has either been studied in space or in laboratory magnetized plasmas other than dipole geometry. In the dipole plasma devices in laboratory, the main experimental findings include high beta plasma confinement<sup>14,15</sup> and inward diffusion<sup>16</sup> in Levitated Dipole Experiment (LDX) at MIT; chaotic particle transport<sup>17</sup>, collisionless radial transport<sup>18</sup> and generation of artificial radiation belt<sup>19</sup> in Collisionless Terrella Experiment (CTX) at Columbia University; vortex formation<sup>20</sup> in Ring Trap-1 (RT-1) at the University of Tokyo; excitation of whistler<sup>21</sup> and chorus<sup>22</sup> waves in Dipole Research Experiment

(DREX) in China; and diffusion induced transport<sup>23</sup>, optical emissivity<sup>24</sup>, anisotropic electrical conductivity<sup>25</sup>, current density profiles<sup>26</sup>, energy distributions<sup>27</sup> and fluctuations<sup>28</sup> in the table top device in our laboratory<sup>29</sup>. Despite this extensive research, to the best of our knowledge, superadiabaticity<sup>3</sup> has neither been observed in the laboratory nor investigated in detail in space.

In this Letter, we report for the first time the experimental observation of superadiabatic electrons in a magnetized laboratory plasma in the presence of heating and anisotropic work done along various directions, incorporating effective dimensionality ( $f^*$ )<sup>30</sup>. Unique to the present study is the local obtainment of superadiabatic polytropic indices, driven by non-resonant heating processes as discussed later.

The experiment has been performed in a compact dipole device, as illustrated in Fig. 2(a). The experimental set-up comprises a spherical vacuum chamber, evacuated to a base pressure of 1  $\mu$ Torr through the combined action of a turbo molecular pump and a dry scroll pump. Argon is used as a test gas. Plasma generation is achieved through electron cyclotron resonance (ECR) heating using waves of 2.45 GHz generated by a magnetron-based microwave generator. The plasma is confined by a permanent cylindrical magnet (NdFeB) of length 4.1 cm and diameter 2.3 cm. The magnet is housed inside a water-cooled holder and is suspended from the top to the center of the experimental chamber (cf. Fig. 2(b)). The magnetic field ( $B$ ) profile of the magnet with  $r$  at  $\theta = 90^\circ$  is shown in Fig. 2(c). The vertical and horizontal solid lines correspond to the radial position (in cm) and magnetic field (in T) where  $\omega_p = \omega_c$ , which is attained at 3.1 cm at  $\theta = 90^\circ$  (cf. Fig. 2(a));  $\omega_p (= N_e e^2 / (m_e \epsilon_0))$  and  $\omega_c (= eB / m_e)$  being the plasma and electron cyclotron frequencies, respectively. Here,  $N_e$  is the measured electron density,  $\epsilon_0$  is the permittivity of free space,  $e$  and  $m_e$  are the electronic charge and mass respectively. The plasma is magnetically confined until  $\sim 20$  cm from the center of the chamber. The confinement is notably stronger until a point ( $r \sim 8$  cm), beyond which the space potential starts to decrease<sup>23,29</sup>. Details of the polar profile of magnetic field intensity and ECR location can be found in Ref.<sup>29,31</sup>. In table I,  $N_e$ , perpendicular and parallel electron temperature ( $T_{e\perp}$  and  $T_{e\parallel}$ ), the characteristic magnetic field scale length ( $|B/\nabla B|$ ), electron Larmor radius ( $r_L (= \sqrt{m_e k_B T_{e\perp}} / eB$ ,  $k_B$  being the Boltzmann constant)) and  $\omega_p / \omega_c$  are tabulated at fixed radial

<sup>a)</sup>ayasha@iitk.ac.in

<sup>b)</sup>sudeepb@iitk.ac.in

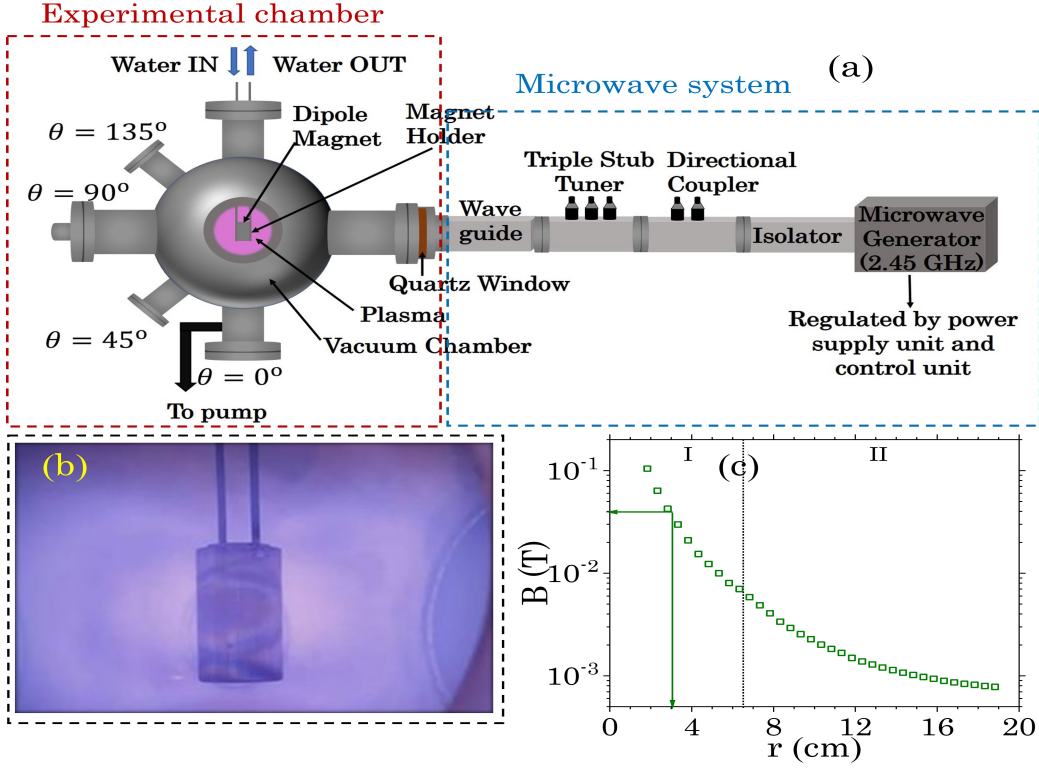


FIG. 2. (a) Schematic of the experimental set-up consisting of the experimental chamber and microwave system. (b) Digital picture of argon plasma confined by a permanent dipole magnet inside the experimental chamber, composed of local thermodynamic systems for the present study. (c) Measured magnetic field strength with radial distance at  $\theta = 90^\circ$  using a Lakeshore 421 gaussmeter with least count of 1 Gauss. Solid lines correspond to the radial location and magnetic field, where plasma frequency is equal to the electron cyclotron frequency.

distances selected from each region: I and II (separated by vertical dashed line in Fig. 2(c) for  $\theta = 90^\circ$ ). The diagnostics used in this work are Langmuir probe with appropriate Bohm<sup>29</sup> and geometric correction<sup>31</sup> to the probe collection area due to the magnetized plasma, and the linear antenna for wave electric field measurements using micro-coax microwave grade RG316 (DC—3 GHz) cables<sup>26</sup>. The measured electric field ( $E'_1$ ) is obtained from the average intensity  $(1/2)\epsilon_0 c E'^2_1 = P/A$ , where  $c$  is the velocity of light,  $P$  is the power detected by the antenna and  $A$  ( $= 4.91 \times 10^{-6} \text{ m}^2$ ) is the area of the antenna. The measured  $E'_1$  is calibrated with a known electric field ( $E_1$ ) inside a cylindrical waveguide with cross-section area  $1.91 \times 10^{-2} \text{ m}^2$  subjected to varying input wave power (300–400 W) at 2.45 GHz frequency in vacuum.  $E_1$  and  $E'_1$  are related as

$$E_1 = (\log E'_1 + 6.51) \times 4.03 \times 10^2 \text{ V/m.} \quad (1)$$

Using this relation, the antennas have been calibrated to obtain the exact microwave electric field inside the plasma.

The operating conditions for the present study are systematically controlled at the pressure of 0.4, 1.2 and 2.0 mTorr and input wave power of 300, 351 and 399 W. Measurements were taken at different polar angles  $\theta = 0^\circ, 45^\circ, 90^\circ$  and  $135^\circ$ , and the results for 1.2 mTorr, 300 W at  $\theta = 90^\circ$  are presented. The construction of the diagnostics and operation details of the experimental system can be found in the works of Nanda *et al*<sup>25,26</sup>.

TABLE I. Electron density ( $N_e$ ), perpendicular and parallel electron temperature ( $T_{e\perp}$  and  $T_{e\parallel}$ ), magnetic field scale length ( $|B/\nabla B|$ ), Larmor radius ( $r_L$ ) and the ratio of plasma frequency ( $\omega_p$ ) to electron cyclotron frequency ( $\omega_c$ ) at fixed radial distances from two regions: I ( $r = 3 \text{ cm}$ ) and II ( $r = 14 \text{ cm}$ ).

r (in cm)	$N_e$ ( $\times 10^{16}$ ) (in $\text{m}^{-3}$ )	$T_{e\perp}$ (in eV)	$T_{e\parallel}$ (in eV)	$ B/\nabla B $ (in cm)	$r_L$ (in cm)	$\omega_p/\omega_c$
3	1.28	4.79	6.29	1.26	0.02	0.86
14	1.72	1.44	1.63	8.73	0.38	37.04

The polytropic index in a plasma can be obtained from<sup>3,30</sup>,

$$\gamma_{\text{lor}\parallel} = 1 + (\gamma_a^* - 1) \left[ 1 - \left( \frac{dQ}{dw} \right)_{\text{lor}\parallel} \right], \quad (2)$$

where  $\perp$  and  $\parallel$  denote the perpendicular and parallel direction to the magnetic field ( $B$ ) respectively,  $dQ$  is the heat supplied to the system,  $dw$  is the work done having positive (or negative) values signifying plasma expansion (or compression) and  $\gamma_a^*$  ( $= 1 + (2/f^*)$ ) is the modified adiabatic index in an anisotropic plasma,  $f^*$  being the effective dimensionality, which depends upon kinetic degrees of freedom  $f$  and anisotropy  $\alpha$  ( $=$

$T_{e\perp}/T_{e\parallel}$ ), given by<sup>30</sup>,

$$f^* = \frac{1 + (f-1)^2 \alpha^2}{1 + (f-1)\alpha^2}, \quad (3)$$

and holds good for  $\alpha < 2$ <sup>30</sup>. In our experiments,  $\alpha$  lies between 0.7–1.7<sup>25</sup> and  $f^*$  varies between 1.49–1.85 for  $f = 3$ . Furthermore, the perpendicular and parallel work in the presence of  $B$  are given by<sup>32,33</sup>,

$$\begin{aligned} dw_{\perp} &= p_{\perp} dV_{\perp} = -p_{\perp} V d(\ln B) \\ \text{and } dw_{\parallel} &= p_{\parallel} dV_{\parallel} = -p_{\parallel} V d\left(\ln \frac{N_e}{B}\right), \end{aligned} \quad (4)$$

respectively, with  $V$  being the elementary flux tube volume. Substituting perpendicular and parallel plasma pressures  $p_{\perp} (= N_e k_B T_{e\perp})$  and  $p_{\parallel} (= N_e k_B T_{e\parallel})$ , and  $V (= N/N_e)$ ,  $N$  being the total number of electrons in Eq. 4, the ratio of net heat supplied to the work done (cf. Eq. 2) can be derived as,

$$\left(\frac{dQ}{dw}\right)_{\perp} = \frac{N(dq_{\perp} - dl_{\perp})}{dw_{\perp}} = -\frac{1}{k_B T_{e\perp}} \frac{(dq_{\perp}/dt - dl_{\perp}/dt)}{d(\ln B)/dt}, \quad (5)$$

and

$$\left(\frac{dQ}{dw}\right)_{\parallel} = \frac{N(dq_{\parallel} - dl_{\parallel})}{dw_{\parallel}} = -\frac{1}{k_B T_{e\parallel}} \frac{(dq_{\parallel}/dt - dl_{\parallel}/dt)}{d(\ln(N_e/B))/dt}, \quad (6)$$

where  $(dq_{\perp\parallel}/dt)$  and  $(dl_{\perp\parallel}/dt)$  are the heating and loss rates per electron respectively. For a plasma at steady-state confined in a static magnetic field,

$$\frac{dq_{\perp}}{dt} = \underbrace{\frac{eE_{1\perp}^2}{2m_e} \frac{v_{h\perp}}{v_{h\perp}^2 + (\omega - \omega_c)^2}}_{W_{M\perp}} + \underbrace{\frac{T_{e\perp}}{B} (\vec{v}_E \cdot \vec{\nabla} B)}_{W_{G\perp}}, \quad (7)$$

$$\frac{dq_{\parallel}}{dt} = \underbrace{\frac{eE_{1\parallel}^2}{2m_e} \frac{v_{h\parallel}}{v_{h\parallel}^2 + (\omega - \omega_c)^2}}_{W_{M\parallel}} + \underbrace{\left(T_{e\parallel} + \frac{m_e}{e} v_{\parallel}^2\right) \vec{v}_E \cdot (\hat{B} \cdot \vec{\nabla} B)}_{W_{C\parallel}}, \quad (8)$$

$$\frac{dl_{\perp}}{dt} = \underbrace{v_{z\perp} \epsilon_z + v_{x\perp} \epsilon_x + v_{h\perp} \frac{3m_e}{M} T_{e\perp}}_{W_{in\perp}} + \underbrace{v_{c\perp} T_{e\perp}}_{W_{cx\perp}} + \underbrace{v_{i\perp} (T_{e\perp} - T_{e\parallel})}_{W_{is\perp}}, \quad (9)$$

$$\frac{dl_{\parallel}}{dt} = \underbrace{v_{z\parallel} \epsilon_z + v_{x\parallel} \epsilon_x + v_{h\parallel} \frac{3m_e}{M} T_{e\parallel}}_{W_{in\parallel}} + \underbrace{v_{c\parallel} T_{e\parallel}}_{W_{cx\parallel}} + \underbrace{v_{i\parallel} (T_{e\parallel} - T_{e\perp})}_{W_{is\parallel}}, \quad (10)$$

where  $E_{1(\perp\parallel)}$  is the wave electric field,  $v_{h(\perp\parallel)}$ ,  $v_{z(\perp\parallel)}$ ,  $v_{x(\perp\parallel)}$ ,  $v_{c(\perp\parallel)}$  and  $v_{i(\perp\parallel)}$  are the electron-neutral collision, ionization, excitation, charge exchange and isotropization

frequencies respectively<sup>34,35</sup>,  $\omega$  is the angular wave frequency,  $v_{\parallel}$  is the fluid velocity obtained by solving the momentum equation along parallel direction<sup>25</sup>,  $M$  is the ionic mass, and  $\epsilon_z$  and  $\epsilon_x$  are the ionization and electronic excitation energies. The loss rate comprises losses due to inelastic  $W_{in(\perp\parallel)}$  and elastic collisions  $W_{el(\perp\parallel)}$ <sup>34</sup>, charge exchange  $W_{cx(\perp\parallel)}$ <sup>29</sup> and isotropization  $W_{is(\perp\parallel)}$ <sup>35</sup>.  $W_{M(\perp\parallel)}$  represents the rate of direct wave-induced heating dependent on its local electric field intensity; from henceforth referred to as wave-induced heating rate<sup>36,37</sup>. Apart from the wave-induced heating, electrons undergoing grad- $B$  and curvature drifts along perpendicular and parallel directions respectively get accelerated by the electric field resulting in net energy gain, hereafter referred to as gradient ( $W_{G\perp}$ ) and curvature ( $W_{C\parallel}$ ) heating rates<sup>38</sup>. In  $W_{G\perp}$  and  $W_{C\parallel}$  (cf. Eq. (7) and (8)),  $\vec{v}_E$  is the  $\vec{E} \times \vec{B}$  drift velocity arising from  $B$  and the total electric field  $\vec{E}(\vec{r}, t) = \vec{E}_0(\vec{r}) + \vec{E}_1(\vec{r}, t)$ , where  $\vec{E}_0(\vec{r})$  is the electrostatic field resulting from the gradient of the space potential and  $\vec{E}_1(\vec{r}, t)$  is the wave electric field<sup>26</sup>. In the present experiment,  $\vec{E} \cong \vec{E}_1$  since  $|\vec{E}_0| \ll |\vec{E}_1|$ , and the drift velocity  $\vec{v}_E$  is primarily governed by  $\vec{E}_1$ . However, situation may arise where  $\vec{E} \cong \vec{E}_0$  when  $\vec{E}_1$  is either absent or weak in comparison to  $\vec{E}_0$ . The derivatives in the denominator of the right hand side of Eq. 5 and 6 can be obtained as,

$$\frac{d(\ln B)}{dt} = \frac{\partial(\ln B)}{\partial t} + v_{\perp} \nabla_{\perp}(\ln B), \quad (11)$$

$$\frac{d(\ln(N_e/B))}{dt} = \frac{\partial(\ln(N_e/B))}{\partial t} + v_{\parallel} \nabla_{\parallel}(\ln(N_e/B)), \quad (12)$$

where  $v_{\perp}$  is the fluid velocity along perpendicular direction<sup>25</sup>. Substituting Eq. (7), (9) and (11) in Eq. (5), and Eq. (8), (10) and (12) in Eq. (6), and then by employing Eq. (5) and (6) in Eq. (2), the perpendicular and parallel polytropic indices can be derived as,

$$\begin{aligned} \gamma_{\perp} &= 1 + (\gamma_a^* - 1) \left[ 1 + \left( \frac{1}{k_B T_{e\perp}} \frac{W_{G\perp}}{v_{\perp} \nabla_{\perp}(\ln B)} \right. \right. \\ &\quad \left. \left. + \frac{1}{k_B T_{e\perp}} \frac{W_{M\perp}}{v_{\perp} \nabla_{\perp}(\ln B)} - \frac{1}{k_B T_{e\perp}} \frac{dl_{\perp}/dt}{v_{\perp} \nabla_{\perp}(\ln B)} \right) \right], \end{aligned} \quad (13)$$

$$\begin{aligned} \gamma_{\parallel} &= 1 + (\gamma_a^* - 1) \left[ 1 + \left( \frac{1}{k_B T_{e\parallel}} \frac{W_{C\parallel}}{v_{\parallel} \nabla_{\parallel} \ln(N_e/B)} \right. \right. \\ &\quad \left. \left. + \frac{1}{k_B T_{e\parallel}} \frac{W_{M\parallel}}{v_{\parallel} \nabla_{\parallel} \ln(N_e/B)} - \frac{1}{k_B T_{e\parallel}} \frac{dl_{\parallel}/dt}{v_{\parallel} \nabla_{\parallel} \ln(N_e/B)} \right) \right]. \end{aligned} \quad (14)$$

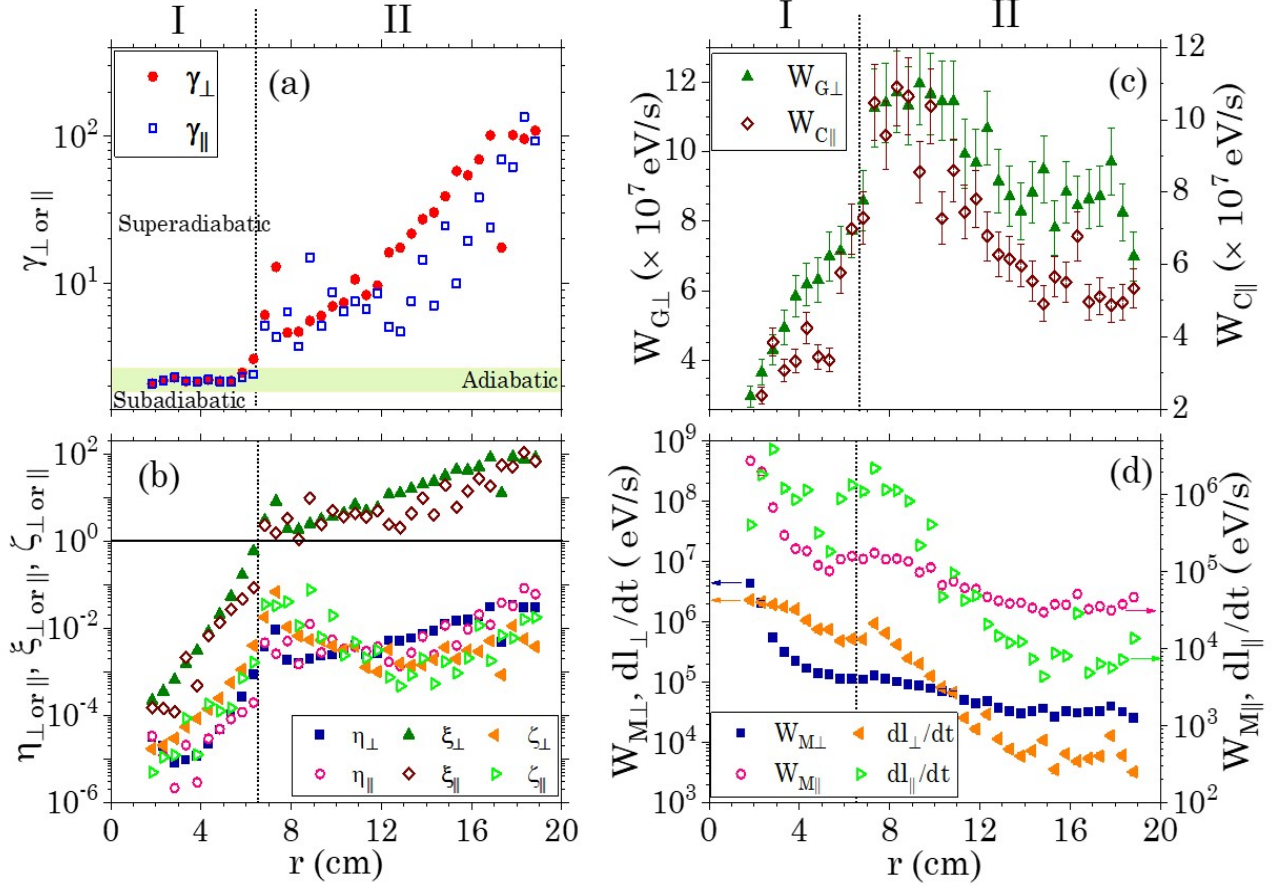


FIG. 3. Radial profiles of (a) polytropic index,  $\gamma_{\perp\text{or}\parallel}$  with the green band denoting the adiabatic region, and (b) ratio of wave-induced heating to the work done,  $\eta_{\perp\text{or}\parallel}$ , ratio of gradient or curvature heating to the work done,  $\xi_{\perp\text{or}\parallel}$  and ratio of energy loss to the work done,  $\zeta_{\perp\text{or}\parallel}$ . The error associated with the standard deviation is within 20% for  $\gamma_{\perp\text{or}\parallel}$ , within 8% for  $\eta_{\perp\text{or}\parallel}$  and  $\xi_{\perp\text{or}\parallel}$ , and within 11% for  $\zeta_{\perp\text{or}\parallel}$ . Variation of (c) gradient,  $W_{G\perp}$  (left y-axis) and curvature,  $W_{C\parallel}$  (right y-axis) heating rates, and (d) perpendicular wave-induced heating rate  $W_{M\perp}$  and energy loss rate  $dl_{\perp}/dt$  (left y-axis) and parallel wave-induced heating rate  $W_{M\parallel}$  and energy loss rate  $dl_{\parallel}/dt$  (right y-axis) with radial distance  $r$  at 1.2 mTorr pressure and 300 W wave power in the equatorial plane ( $\theta = 90^\circ$ ).

Radial profile of  $\gamma_{\perp\text{or}\parallel}$  is plotted in Fig. 3(a) using Eq. 13 and 14. The polytropic index is *nearly adiabatic* ( $\gamma_{\perp\text{or}\parallel} \rightarrow \gamma_a^*$  where  $\gamma_a^* = 1 + (2/f^*) = 1 + (2(1 + 2\alpha^2)/(1 + 4\alpha^2))$ ) for electrons with three kinetic degrees of freedom (cf. Eq. 3) in region I and is *superadiabatic* ( $\gamma_{\perp\text{or}\parallel} > \gamma_a^*$ ) in region II. To understand the superadiabatic nature, radial profiles of the ratio of wave-induced heating to the work done ( $\eta_{\perp\text{or}\parallel}$ ), gradient (or curvature) heating to the work done ( $\xi_{\perp\text{or}\parallel}$ ) and energy losses to the work done ( $\zeta_{\perp\text{or}\parallel}$ ) (cf. Eq. 13 and 14), are plotted in Fig. 3(b) at the same locations and operating conditions, as in Fig. 3(a). The work done along perpendicular and parallel directions is negative as  $dV_{\perp\text{or}\parallel} < 0$  (cf. Eq. 4), and negative work implies plasma compression. Moreover, it is clearly observed that  $\zeta_{\perp\text{or}\parallel}, \eta_{\perp\text{or}\parallel} < \xi_{\perp\text{or}\parallel}$  (cf. Fig. 3(b)), and hence gradient and curvature heating regulates the  $\gamma_{\perp\text{or}\parallel}$  values. Near the magnet ( $r < 6.5$  cm),  $\xi_{\perp\text{or}\parallel} \ll 1$  and  $\gamma_{\perp\text{or}\parallel} \rightarrow \gamma_a^*$ , and in regions at and beyond  $r = 6.5$  cm,  $\xi_{\perp\text{or}\parallel} \geq 1$  resulting in  $\gamma_{\perp\text{or}\parallel} > \gamma_a^*$  (cf. Fig. 3(a) and 3(b)).

To assess the relevance of heating and loss rates with the superadiabatic behavior of electrons, radial profiles of the rate

of gradient ( $W_{G\perp}$ ), curvature ( $W_{C\parallel}$ ), wave-induced ( $W_{M(\perp\text{or}\parallel)}$ ) heating and loss rates ( $dl_{\perp\text{or}\parallel}/dt$ ) are shown in Fig. 3(c) and 3(d). In region II, the heating rates associated with gradient and curvature drifts ( $W_{G\perp}$  and  $W_{C\parallel}$ ) are relatively higher than the wave-induced heating ( $W_{M(\perp\text{or}\parallel)}$ ) and loss rates ( $dl_{\perp\text{or}\parallel}/dt$ ) by a factor of  $\sim 10^2 - 10^4$  and  $\sim 10^2 - 10^3$  in the perpendicular and parallel directions, respectively. This suggests that  $W_{G\perp}$  and  $W_{C\parallel}$  play a crucial role in regulating the net heat supplied to the plasma locally along their respective directions, thereby regulating the values of  $\gamma_{\perp\text{or}\parallel}$ . From the observations, it can be concluded that the superadiabaticity is an outcome of the governance of non-resonant gradient and curvature heating.

In conclusion, this Letter investigates the polytropic index of electrons in a magnetized plasma, taking into account the effects of heating, anisotropic work done, and effective dimensionality arising from temperature anisotropy. The experiment demonstrates local regions with superadiabatic electrons for the first time in a laboratory magnetized plasma. Results indicate that the local superadiabatic electrons are due to heating through acceleration of electrons undergoing grad- $B$

and curvature drifts along perpendicular and parallel directions, respectively, which are intrinsic to magnetized plasma systems with gradients and curvatures in the magnetic field lines<sup>38</sup>. Hence, the results are relevant for planetary magnetosphere with 3-D magnetic bottle structures where particles are trapped<sup>39,40</sup>, undergoing gradient, curvature and  $\vec{E} \times \vec{B}$  drift motion, as well as in solar wind physics<sup>41</sup> and heating mechanisms within solar wind transients<sup>42</sup>. Furthermore, comprehending these heating mechanisms is essential for predicting high-energy particle environments in space, which is crucial for safe space operations and preventing radiation hazards to astronauts<sup>40,42</sup>.

The macroscopic study of the polytropic behavior enhances our understanding of the heating mechanisms in the energy exchange processes. The specific behavior of energy exchange in a superadiabatic system can vary widely based on the nature of the energy sources, associated particle drift velocities, the thermodynamical processes involved, and the plasma system's characteristics. Further, investigation of the thermodynamic properties will be taken up as future work.

## ACKNOWLEDGMENTS

The authors express their gratitude to the funding agency Council of Scientific and Industrial Research (CSIR), India, through Grant No. 03/1496/23/EMR-II. Ayesha Nanda gratefully acknowledges doctoral fellowship under the IN-SPIRE programme (IF180114) of Department of Science & Technology (DST), India.

## AUTHOR DECLARATIONS

### Conflict of interest

The authors have no conflicts to disclose.

## DATA AVAILABILITY

The data that support the findings of this study are available from the corresponding author upon reasonable request.

- <sup>1</sup>D. Frank-Kamenetskii, *Plasma: the fourth state of matter* (Springer Science & Business Media, 2012).
- <sup>2</sup>M. A. Dayeh and G. Livadiotis, "Polytropic behavior in the structures of interplanetary coronal mass ejections," *The Astrophysical Journal Letters* **941**, L26 (2022).
- <sup>3</sup>Z. I. Shaikh, A. N. Raghav, G. Vichare, R. D'Amicis, and D. Telloni, "Evidence for superadiabatic heating and cooling of alfvénic solar wind," *Monthly Notices of the Royal Astronomical Society: Letters* **519**, L62–L67 (2023).
- <sup>4</sup>K. Stasiewicz, "Ion-pressure equations derived from measurements in space," *Physical Review Letters* **95**, 015004 (2005).
- <sup>5</sup>J. M. Little and E. Y. Choueiri, "Electron cooling in a magnetically expanding plasma," *Physical Review Letters* **117**, 225003 (2016).
- <sup>6</sup>K. Takahashi, C. Charles, R. Boswell, and A. Ando, "Adiabatic expansion of electron gas in a magnetic nozzle," *Physical Review Letters* **120**, 045001 (2018).

- <sup>7</sup>K. Dialynas, E. Roussos, L. Regoli, C. P. Paranicas, S. M. Krimigis, M. Kane, D. G. Mitchell, D. C. Hamilton, N. Krupp, and J. F. Carbary, "Energetic ion moments and polytropic index in saturn's magnetosphere using cassini/mimi measurements: A simple model based on  $\kappa$ -distribution functions," *Journal of Geophysical Research: Space Physics* **123**, 8066–8086 (2018).
- <sup>8</sup>T. Wang, L. Ofman, X. Sun, E. Provornikova, and J. M. Davila, "Evidence of thermal conduction suppression in a solar flaring loop by coronal seismology of slow-mode waves," *The Astrophysical Journal Letters* **811**, L13 (2015).
- <sup>9</sup>S. K. Prasad, J. Raes, T. Van Doorselaere, N. Magyar, and D. Jess, "The polytropic index of solar coronal plasma in sunspot fan loops and its temperature dependence," *The Astrophysical Journal* **868**, 149 (2018).
- <sup>10</sup>K. Takahashi, C. Charles, R. W. Boswell, and A. Ando, "Thermodynamic analogy for electrons interacting with a magnetic nozzle," *Physical Review Letters* **125**, 165001 (2020).
- <sup>11</sup>Y. Zhang, C. Charles, and R. Boswell, "A polytropic model for space and laboratory plasmas described by bi-maxwellian electron distributions," *The Astrophysical Journal* **829**, 10 (2016).
- <sup>12</sup>J. Y. Kim, K. Chung, S. Kim, J. H. Ryu, K.-J. Chung, and Y. Hwang, "Thermodynamics of a magnetically expanding plasma with isothermally behaving confined electrons," *New Journal of Physics* **20**, 063033 (2018).
- <sup>13</sup>K. Takahashi, "Helicon-type radiofrequency plasma thrusters and magnetic plasma nozzles," *Reviews of Modern Plasma Physics* **3**, 3 (2019).
- <sup>14</sup>H. Saitoh, Z. Yoshida, J. Morikawa, Y. Yano, T. Mizushima, Y. Ogawa, M. Furukawa, Y. Kawai, K. Harima, Y. Kawazura, Y. Kaneko, K. Tadachi, S. Emoto, M. Kobayashi, T. Sugiura, and G. Vogel, "High- $\beta$  plasma formation and observation of peaked density profile in RT-1," *Nuclear Fusion* **51**, 063034 (2011).
- <sup>15</sup>D. Garnier, A. Hansen, M. Mauel, E. Ortiz, A. Boxer, J. Ellsworth, I. Karim, J. Kesner, S. Mahar, and A. Roach, "Production and study of high-beta plasma confined by a superconducting dipole magnet," *Physics of Plasmas* **13**, 056111 (2006).
- <sup>16</sup>A. Boxer, R. Bergmann, J. Ellsworth, D. Garnier, J. Kesner, M. Mauel, and P. Woskov, "Turbulent inward pinch of plasma confined by a levitated dipole magnet," *Nature Physics* **6**, 207–212 (2010).
- <sup>17</sup>H. Warren and M. Mauel, "Observation of chaotic particle transport induced by drift-resonant fluctuations in a magnetic dipole field," *Physical Review Letters* **74**, 1351 (1995).
- <sup>18</sup>M. E. Mauel, H. H. Warren, and A. Hasegawa, "An experiment to measure collisionless radial transport of energetic electrons confined by a dipole magnetic field," *IEEE transactions on plasma science* **20**, 626–630 (1992).
- <sup>19</sup>M. E. Mauel, "Laboratory observations of wave-induced radial transport within an artificial radiation belt," *Le Journal de Physique IV* **7**, C4–307 (1997).
- <sup>20</sup>Z. Yoshida, H. Saitoh, J. Morikawa, Y. Yano, S. Watanabe, and Y. Ogawa, "Magnetospheric vortex formation: self-organized confinement of charged particles," *Physical Review Letters* **104**, 235004 (2010).
- <sup>21</sup>H. Huang, Z. Wang, X. Tao, and X. Wang, "Simulations on the electron dynamics in excitation of whistler mode waves with dipole research experiment (DREX) parameters," *Physics of Plasmas* **26**, 022106 (2019).
- <sup>22</sup>H. Huang, Z.-B. Wang, X.-G. Wang, and X. Tao, "Excitation of chorus-like waves by temperature anisotropy in dipole research experiment (DREX): A numerical study," *Chinese Physics B* **27**, 015201 (2018).
- <sup>23</sup>A. R. Baitha, A. Nanda, S. Hunjan, and S. Bhattacharjee, "Steady state densities in a plasma confined by a dipole magnet: Diffusion induced transport explored through direct measurements and modeling," *AIP Advances* **10**, 045328 (2020).
- <sup>24</sup>S. Bhattacharjee, A. R. Baitha, J. V. Mathew, and S. Bhattacharjee, "Characterizing spatially varying optical emissions in a steady-state dipole plasma: inversion based experiments and modeling," *Physica Scripta* **96**, 035605 (2021).
- <sup>25</sup>A. Nanda and S. Bhattacharjee, "Temperature anisotropy governed electrical conductivity tensor in a steady state dipole plasma: Spatially resolved experiments and modeling," *Physics of Plasmas* **29**, 062105 (2022).
- <sup>26</sup>A. Nanda and S. Bhattacharjee, "Current density profiles in a compact dipole plasma," *Physics of Plasmas* **30**, 052107 (2023).
- <sup>27</sup>S. Hunjan and S. Bhattacharjee, "Measurement of electron energetics in the equatorial and polar planes of a compact dipole plasma driven at steady state," *Plasma Sources Science and Technology* **32**, 105018 (2023).

- <sup>28</sup>S. Hunjan and S. Bhattacharjee, “Characteristics of fluctuations in the equatorial and polar directions of a compact dipole plasma driven at steady state,” *Physics of Plasmas* **31**, 092106 (2024).
- <sup>29</sup>S. Bhattacharjee, A. R. Baitha, A. Nanda, S. Hunjan, and S. Bhattacharjee, “Physics of plasmas confined by a dipole magnet: insights from compact experiments driven at steady state,” *Reviews of Modern Plasma Physics* **6**, 16 (2022).
- <sup>30</sup>G. Livadiotis and G. Nicolaou, “Relationship between polytropic index and temperature anisotropy in space plasmas,” *The Astrophysical Journal* **909**, 127 (2021).
- <sup>31</sup>A. R. Baitha, A. Nanda, S. Hunjan, and S. Bhattacharjee, “Particle balance in a steady state plasma in a dipole magnetic field,” *Plasma Research Express* **1**, 045005 (2019).
- <sup>32</sup>S. Du, G. P. Zank, X. Li, and F. Guo, “Energy dissipation and entropy in collisionless plasma,” *Physical Review E* **101**, 033208 (2020).
- <sup>33</sup>X. Guo, L. Sironi, and R. Narayan, “Electron heating in low-mach-number perpendicular shocks. I. Heating mechanism,” *The Astrophysical Journal* **851**, 134 (2017).
- <sup>34</sup>S. Pandey, D. N. Patel, A. R. Baitha, and S. Bhattacharjee, “Particle energy distributions and metastable atoms in transient low pressure interpulse microwave plasma,” *Plasma Sources Science and Technology* **24**, 065004 (2015).
- <sup>35</sup>Y. Kawazura, Z. Yoshida, M. Nishiura, H. Saitoh, Y. Yano, T. Nogami, N. Sato, M. Yamasaki, A. Kashyap, and T. Mushiake, “Observation of particle acceleration in laboratory magnetosphere,” *Physics of Plasmas* **22**, 112503 (2015).
- <sup>36</sup>S. Bhattacharjee, H. Amemiya, and Y. Yano, “Plasma buildup by short-pulse high-power microwaves,” *Journal of Applied Physics* **89**, 3573–3579 (2001).
- <sup>37</sup>S. Bhattacharjee, I. Dey, A. Sen, and H. Amemiya, “Quasisteady state interpulse plasmas,” *Journal of Applied Physics* **101** (2007).
- <sup>38</sup>J. M. TenBarge, J. Juno, and G. G. Howes, “Electron energization in reconnection: Eulerian vs lagrangian perspectives,” *Physics of Plasmas* **31**, 022901 (2024).
- <sup>39</sup>K. Nykyri, A. Otto, E. Adamson, E. Kronberg, and P. Daly, “On the origin of high-energy particles in the cusp diamagnetic cavity,” *Journal of Atmospheric and Solar-Terrestrial Physics* **87**, 70–81 (2012).
- <sup>40</sup>K. Nykyri, C. Chu, X. Ma, S. A. Fuselier, and R. Rice, “First MMS observation of energetic particles trapped in high-latitude magnetic field depressions,” *Journal of Geophysical Research: Space Physics* **124**, 197–210 (2019).
- <sup>41</sup>K. Sorathia, V. Merkin, A. Ukhorskiy, R. Allen, K. Nykyri, and S. Wing, “Solar wind ion entry into the magnetosphere during northward IMF,” *Journal of Geophysical Research: Space Physics* **124**, 5461–5481 (2019).
- <sup>42</sup>B. Burkholder, K. Nykyri, and X. Ma, “Magnetospheric multiscale statistics of high energy electrons trapped in diamagnetic cavities,” *Journal of Geophysical Research: Space Physics* **126**, A028341 (2021).